AIAA JOURNAL
Vol. 45, No. 7, July 2007

Wake-Structure Formation of a Heaving Two-Dimensional Elliptic Airfoil

K. B. Lua,* T. T. Lim,† and K. S. Yeo†
National University of Singapore, Singapore 119260, Republic of Singapore
and
G. Y. Oo‡
DSO National Laboratories, Singapore 118230, Republic of Singapore

DOI: 10.2514/1.25310

This paper is prompted by a recent numerical study (Lewin, G. C., and Haj-Hariri, H., "Modelling Thrust Generation of a Two-Dimensional Heaving Airfoil in Viscous Flow," *Journal of Fluid Mechanics*, Vol. 492, Oct. 2003, pp. 339–362) that shows that for a two-dimensional (2-D) elliptic airfoil undergoing prescribed heaving motion in a viscous fluid, both leading-edge vortices and trailing-edge vortices contributed to the formation of the wake structures. However, an earlier dye-visualization study (Lai, J. C. S., and Platzer, M. F., "Jet Characteristics of a Plunging Airfoil," *AIAA Journal*, Vol. 37, No. 12, 1999, pp. 1529–1537) on a heaving NACA 0012 airfoil appears to show that the wake structures were derived from trailing-edge vortices only. The dissimilarity in the two studies remains unclear because there is no corresponding experimental data on a 2-D heaving elliptic airfoil. In this study, digital particle image velocimetry technique was used to investigate the wake-structure formation of a 2-D elliptic airfoil undergoing simple harmonic heaving motion. For the range of flow conditions investigated here, our results show that the type of wake structures produced is controlled by when and how the leading-edge vortices interact with the trailing-edge vortices.

Nomenclature

A	=	heaving amplitude
c	=	chord length, 20 mm (reference length)
f	=	heaving frequency
h	=	A/c
k	=	$2\pi fc/U_\infty$
kh	=	$2\pi fA/U_\infty$
L	=	length of airfoil, 200 mm
Re	=	$U_\infty c/\nu$
Sta	=	advance ratio, fA/U_∞
Stc	=	reduced frequency, fc/U_∞
T	=	heaving period
t	=	time
U_∞	=	freestream velocity (reference speed)
Y	=	heaving motion
ν	=	kinematic viscosity

I. Introduction

BIOLOGICAL fliers and swimmers, such as insects and fishes, use flapping foils to generate high lift and thrust in fluids. The earliest studies on flapping foils were carried out independently by Knoller [1] and Betz [2], who recognized that a flapping foil generates an effective angle of attack, with the resulting normal force producing both lift and thrust components. This finding was verified by Katzmayr [3], who measured the thrust of a stationary airfoil subjected to a sinusoidally oscillating freestream. A subsequent analysis by Glauert [4] using classical linear theory of an oscillating wing in an inviscid incompressible fluid found that for a fixed advance ratio, there is no preferred frequency, and the thrust coefficient and efficiency increased monotonically with decreasing frequency. A later analysis by Garrick [5] on plunging and pitching plates, based on the assumption of small-amplitude oscillations in an inviscid incompressible fluid, found a rapid reduction in the propulsive efficiencies of flapping foils, from a value of 1.0 at a low flapping frequency to about 0.5 as the frequency is increased. This finding was later confirmed in an experiment by Silverstein and Joyner [6] in 1939. However, von Kármán and Burgers [7] were the first to provide theoretical explanation of drag and thrust production based on the orientation of the wake vortices; the well-known drag-producing Kármán vortex street and thrust-producing reverse Kármán vortex street were identified by them and were later verified experimentally by Bratt [8]. Further theoretical works by Wu [9] and Lighthill [10] showed that flapping foils can generate different kinds of spatially periodic patterns of vortices that were used as a form of propulsion by aquatic animals (see also [11–15]). In the following decades, numerous theoretical and experimental studies [16–28] were conducted to better understand flapping-foil aerodynamics and propulsion, and the recent interest in using flapping wings [29–40] to generate lift and propulsion in applications such as micro air vehicles has given research in this area a further impetus.

Although the bulk of the investigations on flapping foils were concentrated on pure pitching or combined heaving and pitching motions, some studies have also been conducted on pure heaving motion. It is well established that the motion of a heaving airfoil is described by three nondimensional parameters: namely, Sta, Stc, and Re, although in some cases, A/c is used in place of Sta. Depending on the heaving frequency and amplitude, studies by Freymuth [16], Jones et al. [23], Lai and Platzer [24], Lewin and Haj-Hariri [25], and Young and Lai [26] showed that the wake structures of a heaving airfoil can be characterized by a drag-producing Kármán vortex street, thrust-producing reverse Kármán vortex street, or neutral wake (in which two vortices of the same sign are produced in every half-cycle). In a numerical study by Lewin and Haj-Hariri [25] (henceforth referred to as LH) on a heaving two-dimensional (2-D) elliptic airfoil in a viscous fluid, the

Received 19 May 2006; revision received 23 February 2007; accepted for publication 17 March 2007. Copyright © 2007 by the American Institute of Aeronautics and Astronautics, Inc. All rights reserved. Copies of this paper may be made for personal or internal use, on condition that the copier pay the $10.00 per-copy fee to the Copyright Clearance Center, Inc., 222 Rosewood Drive, Danvers, MA 01923; include the code 0001-1452/07 $10.00 in correspondence with the CCC.

*Research Fellow, Department of Mechanical Engineering, 10 Kent Ridge Crescent.
†Associate Professor, Department of Mechanical Engineering, 10 Kent Ridge Crescent.
‡Member of the Technical Staff, 20 Science Park Drive.

wake structures were found to be produced from the interaction of leading-edge vortices (LEVs) and trailing-edge vortices (TEVs); however, an earlier dye-visualization study by Lai and Platzer [24] (henceforth referred to as LP) on a heaving NACA 0012 airfoil showed that these wake structures originated from only the trailing edge of the airfoil. Although the interaction of the LEVs and the TEVs to produce different wake structures in a pitching airfoil is well established, there appears to be a lack of experimental data on a pure heaving 2-D elliptic airfoil to compare with the computational results of LH.

The objective of this study is to examine the wake-structure formation of a 2-D elliptic airfoil undergoing a sinusoidal heaving motion at a constant Reynolds number (based on freestream velocity and the chord length of the airfoil) of about 1000; with the advance ratios of 0.0919, 0.160, and 0.276; and the reduced frequency from 0.1 to 2.0. Our attention is focused on the formation of the large-scale wake structures only (such as the leading-edge and trailing-edge vortices) and not the small-scale structures (such as the boundary-layer and secondary vortices). Previous experimental studies [41–44] showed that the small-scale structures have insignificant influence on the topology of the large-scale structures. Although our Reynolds number is twice that of LH [25], the choice is constrained by our experimental setup. Nevertheless, previous experimental studies [18,19] on an oscillating and translating airfoil showed that Reynolds number has little effect on the wake pattern.

II. Experimental Setup

The experiments were conducted in the recirculating water channel (see Fig. 1) in the Fluid Mechanics Laboratory of the National University of Singapore. The test rig, equipped with a flapping mechanism, was placed inside the test section of the water channel. The flapping mechanism consisted of two servomotors that controlled the pitching and heaving motions of the airfoil with the resolutions of 0.1 mm and 0.025 deg, respectively. In the present study, the pitching motion was not activated. A two-dimensional elliptic airfoil, with a chord length of 20 mm and a maximum thickness of 2.5 mm, spanned the width of the test rig (200-mm wide, giving $L/c = 10$), bounded by two vertical Perspex end plates to reduce three-dimensional flow effects. A third Perspex plate was placed horizontally on the water surface to prevent free surface effects. The airfoil was supported by a brass rod through a vertical slot in the Perspex end plate at the far side of the test section, and the slot was sealed with a flexible rubber flap to prevent flow leakage through the slot. The airfoil was subjected to a sinusoidal heaving motion at a constant Reynolds number of about 1000. The heaving motion was governed by the following equation:

$$Y = A[\cos(2\pi f t)]$$

For digital particle image velocimetry (DPIV) measurements, the flow was uniformly seeded with 10-μm spherical glass particles of a

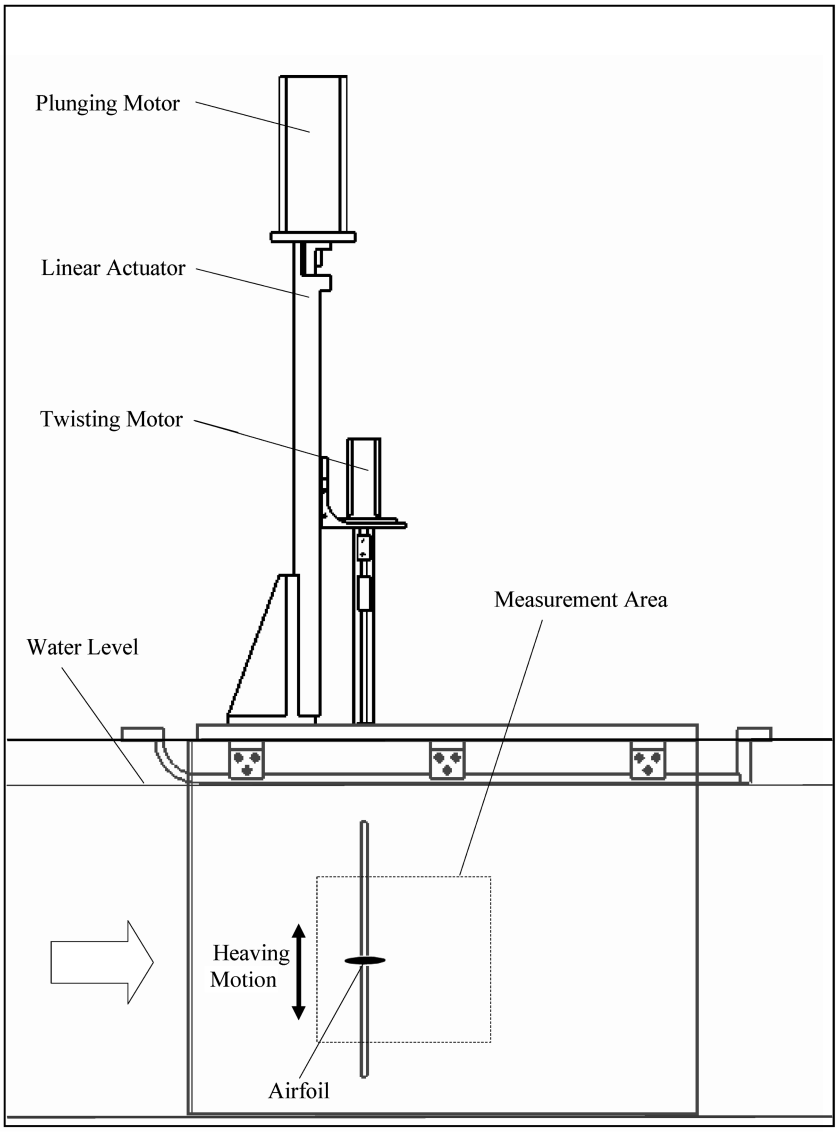

Fig. 1 Side view of the test rig equipped with a flapping mechanism.

density of 1000 ± 20 kg/m^3. The DPIV setup consisted of a server, a dual-cavity Nd-Yag laser, a 1024 by 1024 pixel particle image velocimetry (PIV) camera and a dual-processor CPU Windows NT workstation running Dantec FlowManager Version 3.30 software. The two servomotors that controlled the airfoil pitching and heaving motions were in turn controlled by two National Instruments real-time data-acquisition cards. As pointed out earlier, only the heaving motion was activated in the present experiment. At the start of each run, a program written on LabVIEW calculated the prescribed positional displacement of the airfoil with respect to time, and the NI-DAQ card then sent out the positional signals to the servomotor to start the heaving motion of the airfoil. At the same time, the card triggered the PIV server to start firing the Nd-Yag laser. The laser beam was expanded by a cylindrical lens into a laser sheet 2-mm thick that bisected the span of the airfoil. The PIV server, which controlled the synchronization of the PIV camera and the PIV lasers, signaled the camera to capture image pairs that were recorded as 1008 by 1016 pixel images, corresponding to a physical area of 130.9 by 131.9 mm. On average, more than five particles were captured within the interrogation area of 16×16 pixels. Dantec's adaptive cross-correlation DPIV algorithm was used to analyze the captured flow images. With the preceding interrogation area and 25% overlap in the final step of the processing, the algorithm produced velocity-vector fields with a spatial resolution of $0.1c$. Subpixel accuracy in the velocity vectors was achieved using a three-point symmetrical Gaussian curve-fit interpolation scheme. Data validation was carried out using both peak validation and moving-average validation techniques, and velocity vectors were rejected unless all the criteria were met. The averaged error per interrogation cell in the vorticity calculations, based on the simple difference scheme adopted in the Dantec algorithm, is approximately 6.75% (see also Luff et al. [45]). Estimation based on Cohn and Koochesfahani [46] showed that the resolution of the measurements is sufficient to capture the large-scale wake structures.

A total of 18 heaving motions were conducted through a combination of *Sta* values of 0.0919, 0.160, and 0.276 and *Stc* values of 0.10, 0.25, 0.50, 0.75, 1.00, and 2.00. For each flow condition, the airfoil started and ended its sinusoidal motion of six cycles at its topmost position, and the experiment was repeated a total of 20 runs for subsequent ensemble averaging. Because of the opacity of the airfoil, the laser beam cast a shadow beneath the airfoil, making the shadow region void of data. To circumvent this problem so that a complete flowfield was obtained, every set of the experiment was repeated with the reversed orientation and motion of the airfoil.

III. Results and Discussion

A. Leading-Edge Vortex and Wake Structures

The results obtained in the present study are presented in Figs. 2–11. In agreement with the computations of LH [25], our results show that the type of wake structures produced in a heaving 2-D elliptic airfoil depends very much on when and how the leading-edge vortices interact with the trailing-edge vortices (and sometimes with the airfoil). In general, both LEVs and TEVs are generated at the beginning of each stroke, and they grow and eventually shed as the airfoil moves away, but under some conditions, there is a considerable delay in the shedding of the LEV relative to the TEV. The delay causes a substantial phase shift between the two vortices, which obviously influences the topology of the wake structures. At low reduced frequencies of 0.10 and 0.25, a leading-edge vortex is shed before the end of each stroke, whereas at higher reduced frequencies of 0.50 to 2.00, the LEV is shed at the end of the stroke. For a fixed reduced frequency, the advance ratio controls the amplitude of the motion. In general, the higher the advance ratio (i.e.,

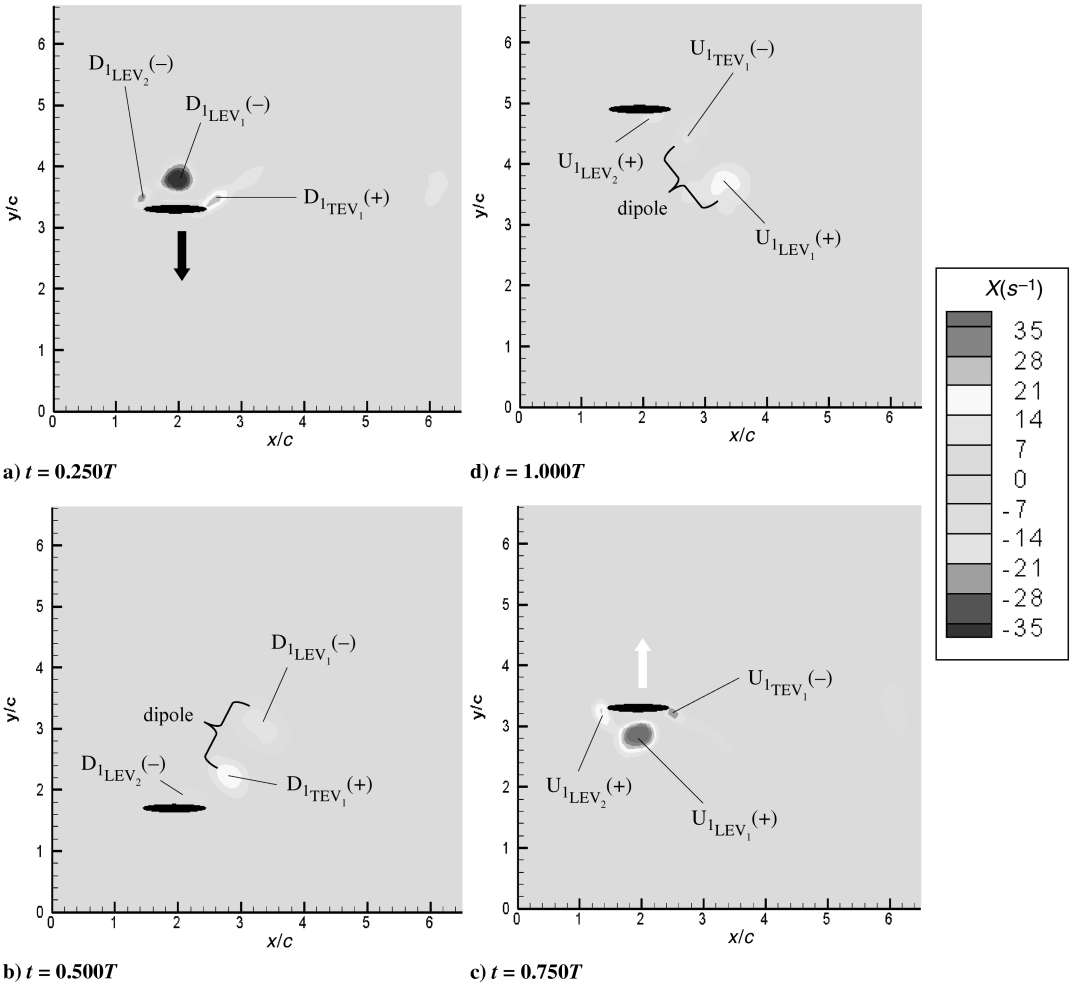

a) $t = 0.250T$ **d)** $t = 1.000T$

b) $t = 0.500T$ **c)** $t = 0.750T$

Fig. 2 Vorticity plot of *Sta* = 0.16 (*h* = 1.6) and *Stc* = 0.1 over one cycle of heaving motion (dissipated wake).

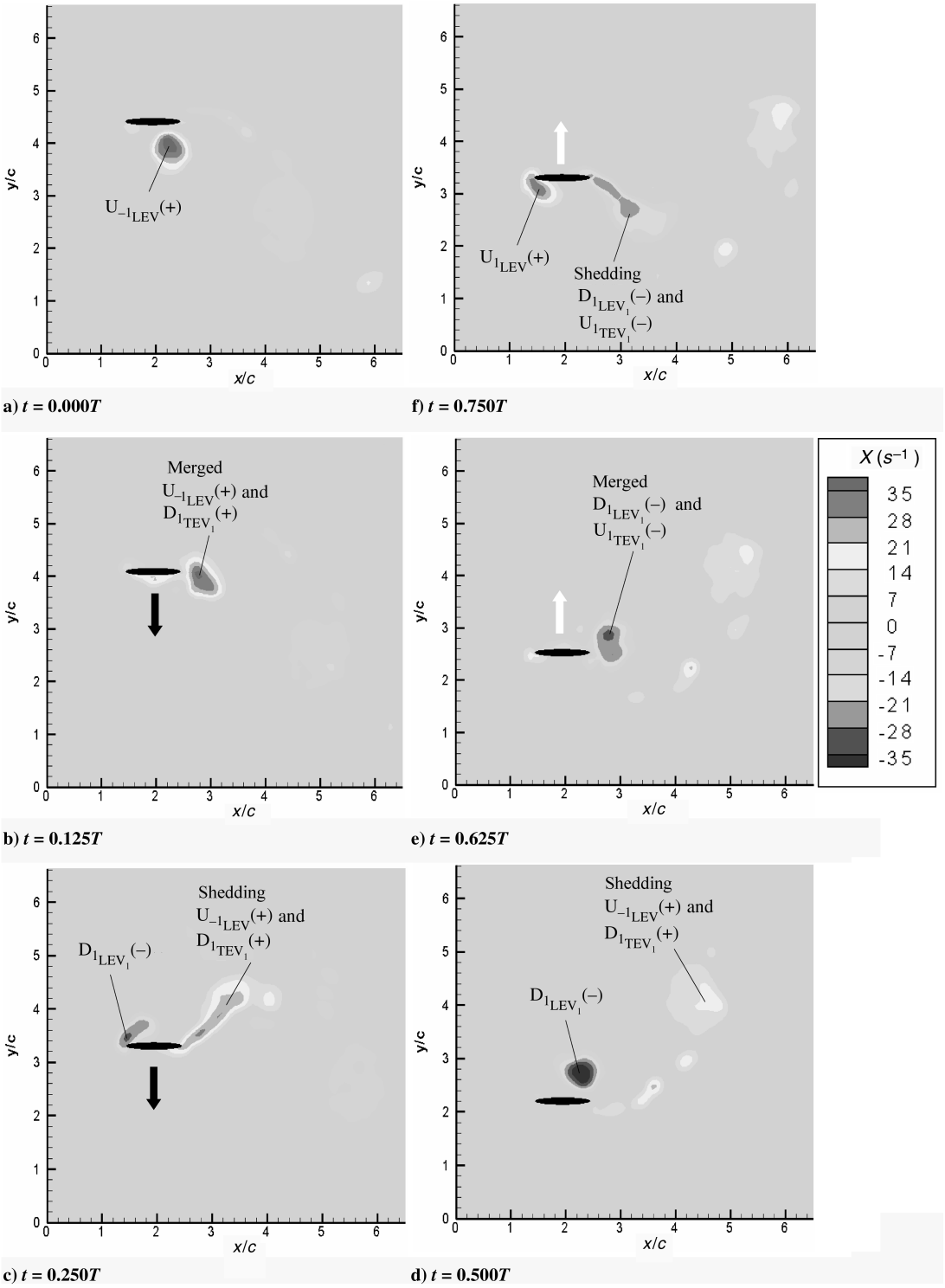

Fig. 3 Vorticity plot of $Sta = 0.276$ ($h = 1.104$) and $Stc = 0.25$ over one cycle of heaving motion (reverse-Kármán-vortex-street-like structure).

higher heaving velocity) the stronger the LEVs and TEVs, but with the tendency of LEV shedding before the airfoil reverses its direction of motion. The following is a summary of the wake patterns observed here.

1) Dissipation wake refers to the absence of coherent vortical structures in the wake region. Here, both the LEV and the TEV, upon shedding from the airfoil, form a dipole that interacts destructively with the freestream. This usually occurs at low Stc of 0.10. We are not aware if this pattern has been observed previously, although the formation of a dipole is not new.

2) A reverse-Kármán-vortex-street-like structure is associated with thrust production and occurs when LEVs and TEVs interact in such a way that two rows of alternating vortices are formed, with the top-row vortices having a counterclockwise circulation and the bottom-row vortices having a clockwise circulation.

3) Deflected wakes are those with the flow structures deflected away from the freestream direction. They occur at the highest reduced frequencies of $Stc = 2.00$ for both the advance ratios $Sta = 0.160$ and 0.276, and $Stc = 1.00$ for $Sta = 0.276$. These wake structures were seen in the past (for example, see LP [24] and LH [25]).

4) Neutral wake structures possess two vortices of equal sign shed every half-cycle. These wake structures have also been seen by LP [24] and LH [25].

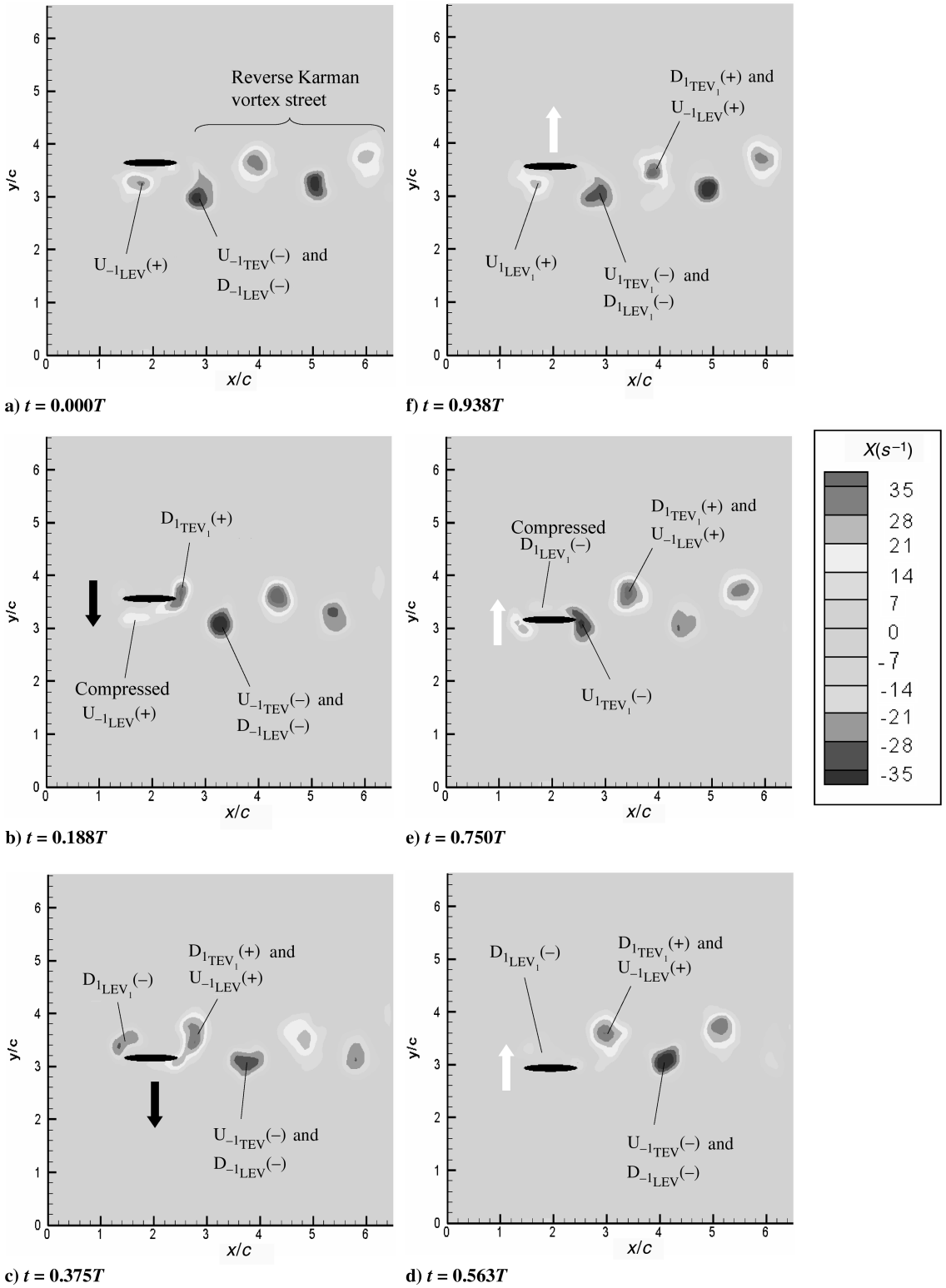

Fig. 4 Vorticity plot of $Sta = 0.276$ ($h = 0.368$) and $Stc = 0.75$ over one cycle of heaving motion (reverse-Kármán-vortex-street-like structure).

5) A merged Kármán vortex street is associated with drag production, and is similar in appearance to the reverse-Kármán-vortex-street-like structure, except for the reversal in the sign of the circulation of the top- and bottom-row vortices.

B. Detailed Description

The vorticity field for each of the preceding cases is presented in Figs. 2–10. Take note that these results were obtained during the fifth cycle of the heaving motion, in which the wake structures behind the airfoil had reached a periodic state. For ease of reference, the vortices of interest are identified by the heaving stroke that they originate from (D for downstroke, U for upstroke, subscript 1 for the current stroke, subscript −1 for the previous stroke, etc.) and the sign of circulation is indicated as either positive (counterclockwise) or negative (clockwise). For example, $D_{1_{LEV_1}}$ (−) signifies current downstroke and first leading-edge vortex with clockwise circulation, and $D_{1_{LEV_2}}$ (−) current downstroke and second leading-edge vortex with clockwise circulation. Likewise, $U_{1_{LEV_1}}$ (+) signifies current upstroke and first leading-edge vortex with counterclockwise

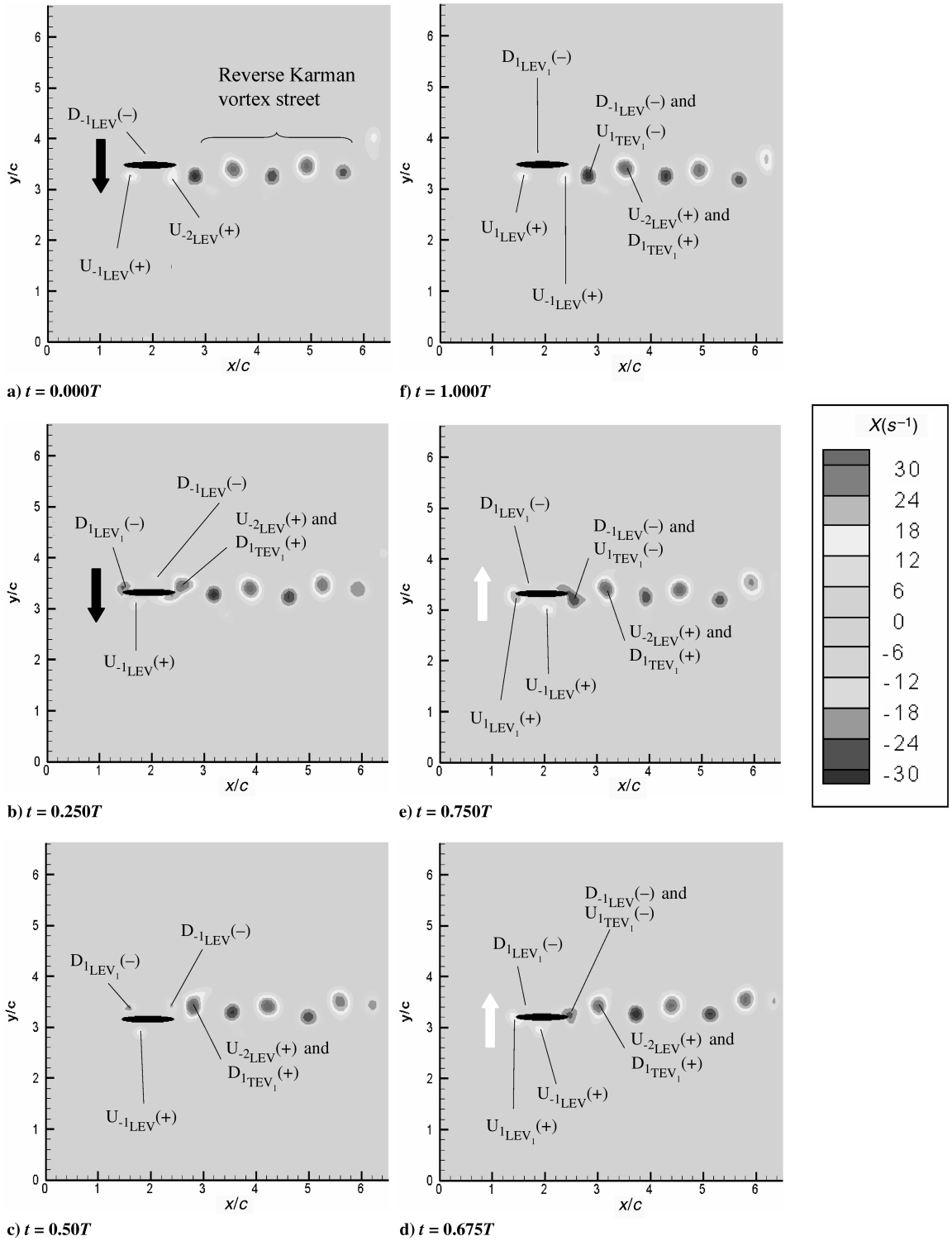

Fig. 5 Vorticity plot of $Sta = 0.16$ ($h = 0.16$) and $Stc = 1$ over one cycle of heaving motion (reverse-Kármán-vortex-street-like structure).

circulation, and $U_{1_{TEV_1}}$ (−) current upstroke and first trailing-edge vortex with clockwise circulation. Similarly, $D_{-1_{LEV}}$ (+) indicates the leading-edge vortex of the previous downstroke.

1. Dissipated Wakes

Figure 2 shows the generation of dissipated wake structures at $Sta = 0.160$ and the lowest Stc of 0.10. As depicted in the figure, the airfoil started with a downstroke motion in which a leading-edge vortex [$D_{1_{LEV_1}}(-)$] was formed and grew as the airfoil moved downward. At about the same time, the shear layer at the trailing edge started to roll up to form $D_{1_{TEV_1}}(+)$ and convected downstream. As soon as $D_{1_{LEV_1}}(-)$ was shed from the leading edge at midstroke (see $t = 0.25$T), a second leading-edge vortex [$D_{1_{LEV_2}}(-)$] was initiated. When $D_{1_{LEV_1}}(-)$ was moving toward the trailing edge, it paired up with $D_{1_{TEV_1}}(+)$ to form a dipole, with the horizontal component of their induced velocity pointed in the upstream direction. During the upstroke motion, a corresponding event occurred, as can be seen in Figs. 2c and 2d. Unlike the other wake structures (which will be discussed later) in which coherent vortices persisted for a greater streamwise distance, the interaction of the dipole with the surrounding flow appears to speed up the annihilation of the vorticity, hence the name "dissipated wakes."

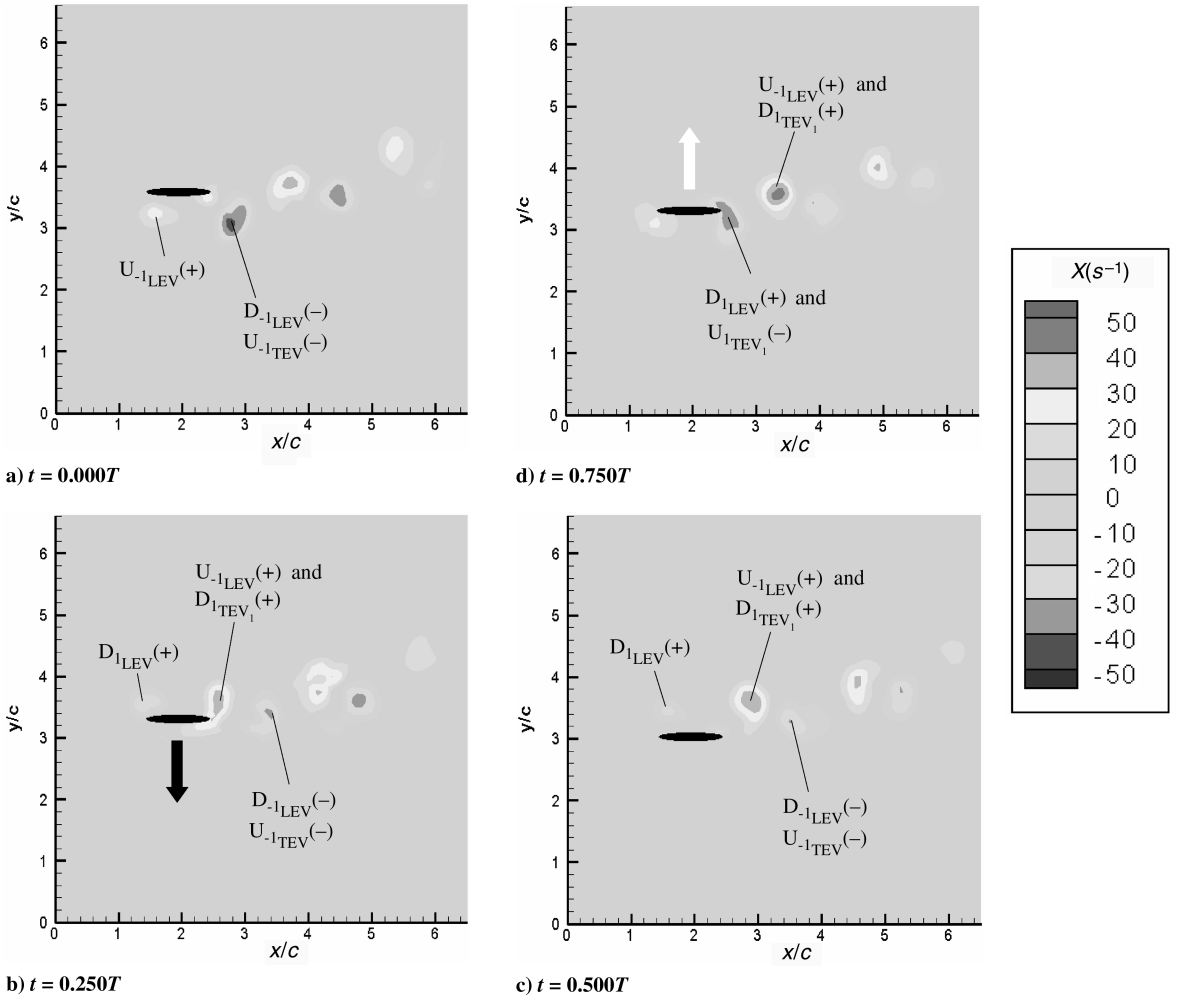

Fig. 6 Vorticity plot of $Sta = 0.276$ ($h = 0.276$) and $Stc = 1$ over one cycle of heaving motion (deflected wake).

2. Reverse-Kármán-Vortex-Street-Like Structure

With increasing Stc, a thrust-producing reverse-Kármán-vortex-street-like structure appeared. Figure 3 shows the result at $Stc = 0.25$ and $Sta = 0.276$. At the beginning of the downstroke ($t = 0.000$), the leading-edge vortex that was formed during the previous upstroke [$U_{-1_{LEV}}(+)$] had already reached the trailing edge. As the airfoil moved downward, at about $t = 0.125T$, $U_{-1_{LEV}}(+)$ was shed from the trailing edge and merged with a new TEV to form $U_{-1_{LEV}}(+) + D_{1_{TEV_1}}(+)$. At about the same time, a new leading-edge vortex [$D_{1_{LEV_1}}(-)$] was initiated. By the time the airfoil had reached the end of the downstroke (see $t = 0.500T$), $D_{1_{LEV_1}}(-)$ had shed and convected toward the trailing edge of the airfoil. As the airfoil reversed its direction of motion and moved upward, $D_{1_{LEV_1}}(-)$ merged with a trailing-edge vortex $U_{1_{TEV_1}}(-)$ of the same circulation [i.e., $D_{1_{LEV_1}}(-) + U_{1_{TEV_1}}(-)$]. Therefore, every stroke of the heave motion created merged vortices at the trailing edge, but with alternating signs, leading to two strong vortices of opposite sign per cycle, and the arrangement of the vortices is such that they formed a reverse-Kármán-vortex-street-like structure, with the top-row vortices having a counterclockwise circulation and the bottom-row vortices having a clockwise circulation.

At a higher value of $Stc = 0.75$, the mechanism leading to the formation of the reverse-Kármán-vortex-street-like structure is the same as before. However, the strength of the merged vortices is slightly weaker. Figure 4 shows the result at $Sta = 0.276$ and $Stc = 0.75$. Here, at the beginning of the downstroke ($t = 0.000$), the LEV formed during the upstroke of the previous cycle $U_{-1_{LEV}}(+)$ was still attached to the airfoil at about a quarter-hord from the leading edge. As the airfoil continued its downward motion with a higher velocity because of a higher Stc (see $t = 0.188T$ and $0.375T$), it compressed $U_{-1_{LEV}}(+)$ with some stretching as the vortex was convecting toward the trailing edge. Therefore, the vorticity of the $U_{-1_{LEV}}(+)$ was partially weaken by the induced secondary vorticity of the opposite sign, in a manner similar to that in an accelerated flow past a NACA 015 airfoil [47]. The weaker $U_{-1_{LEV}}(+)$ subsequently merged with the trailing-edge vortex $D_{1_{TEV_1}}(+)$ of the same sign. The combined strength of $D_{1_{TEV_1}}(+) + U_{-1_{LEV}}(+)$ is now weaker than in the preceding case (Fig. 3), in which no partial annihilation of $U_{-1_{LEV}}(+)$ took place.

When Stc was increased to 1.00 with $Sta = 0.0919$ and 0.160, as a consequence of shorter distances of separation between the shed vortices and the higher heaving frequency, the LEV formed from the previous cycle reached the trailing edge only at the end of the following heaving cycle, as can be seen in Fig. 5 for the case of $Sta = 0.160$ at $Stc = 1.00$. Here, it can be seen that at the beginning of the downstroke ($t = 0.000$), two LEVs [$U_{-2_{LEV}}(+)$ and $U_{-1_{LEV}}(+)$] were on the lower airfoil surface and one [$D_{-1_{LEV}}(-)$] was on the upper surface. When the airfoil began to move downward, both $U_{-1_{LEV}}(+)$ and $D_{-1_{LEV}}(-1)$ convected toward the trailing edge, whereas $U_{-2_{LEV}}(+)$ had started to merge with a newly generated TEV [i.e., $U_{-2_{LEV}}(+) + D_{1_{TEV_1}}(+)$; see $t = 0.250T$]. At the end of the downstroke ($t = 0.500T$), the merged $U_{-2_{LEV}}(+) + D_{1_{TEV_1}}(+)$ had moved away from the trailing edge, and $D_{-1_{LEV}}(-)$ had almost reached the trailing edge. And as the airfoil reversed its direction of motion and moved up, $D_{-1_{LEV}}(-)$ merged with a new TEV [i.e., $D_{-1_{LEV}}(-) + U_{1_{TEV_1}}(-)$; see $t = 0.675T$]. Although $U_{-1_{LEV}}(+)$ and $D_{1_{LEV}}(-)$ were convecting along the upper and lower airfoil surfaces, respectively, a new LEV [$U_{1_{LEV_1}}(+)$] started to form at the leading

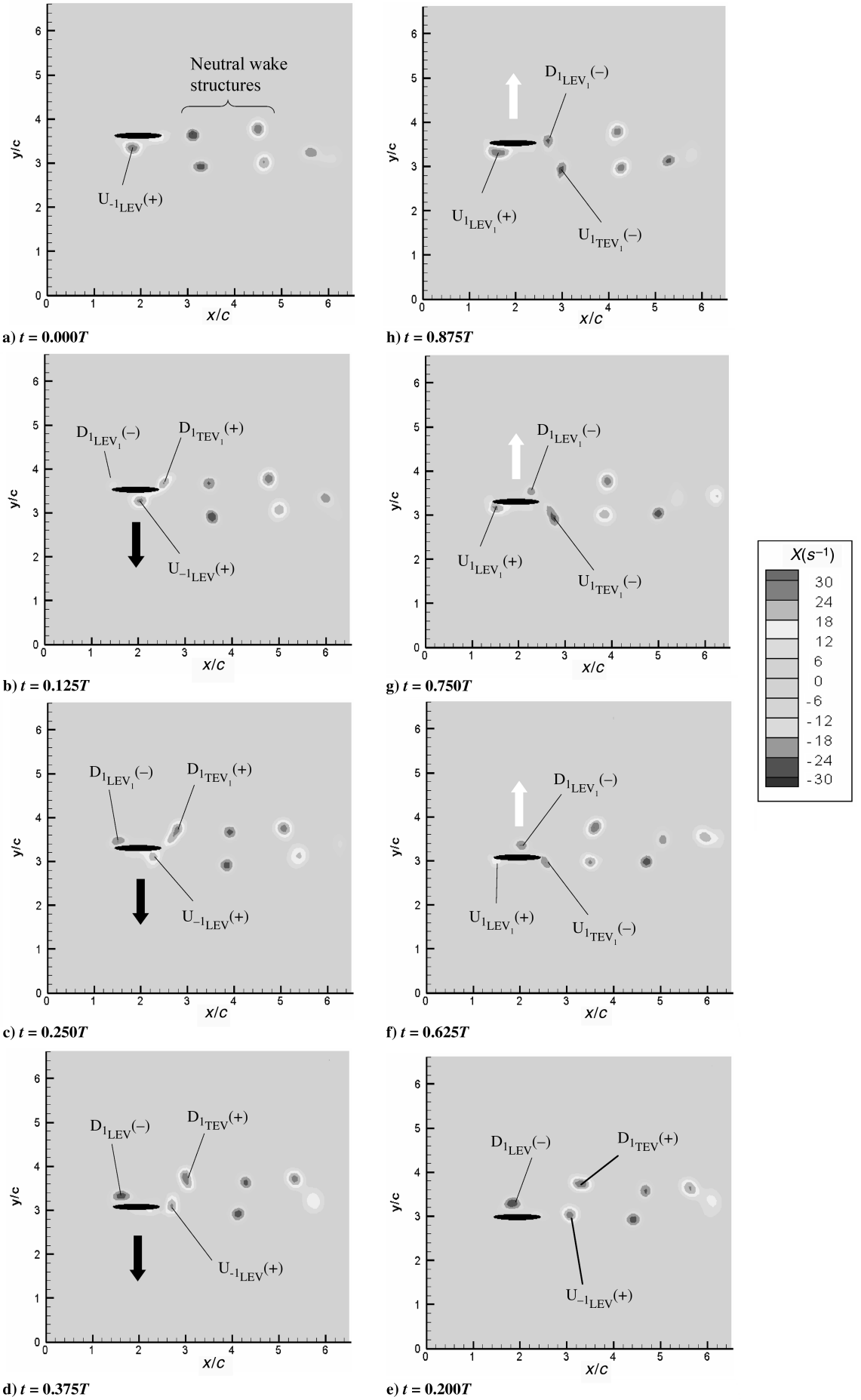

a) $t = 0.000T$ h) $t = 0.875T$

b) $t = 0.125T$ g) $t = 0.750T$

c) $t = 0.250T$ f) $t = 0.625T$

d) $t = 0.375T$ e) $t = 0.200T$

Fig. 7 Vorticity plot of $Sta = 0.16$ ($h = 0.32$) and $Stc = 0.5$ over one cycle of heaving motion (neutral wake).

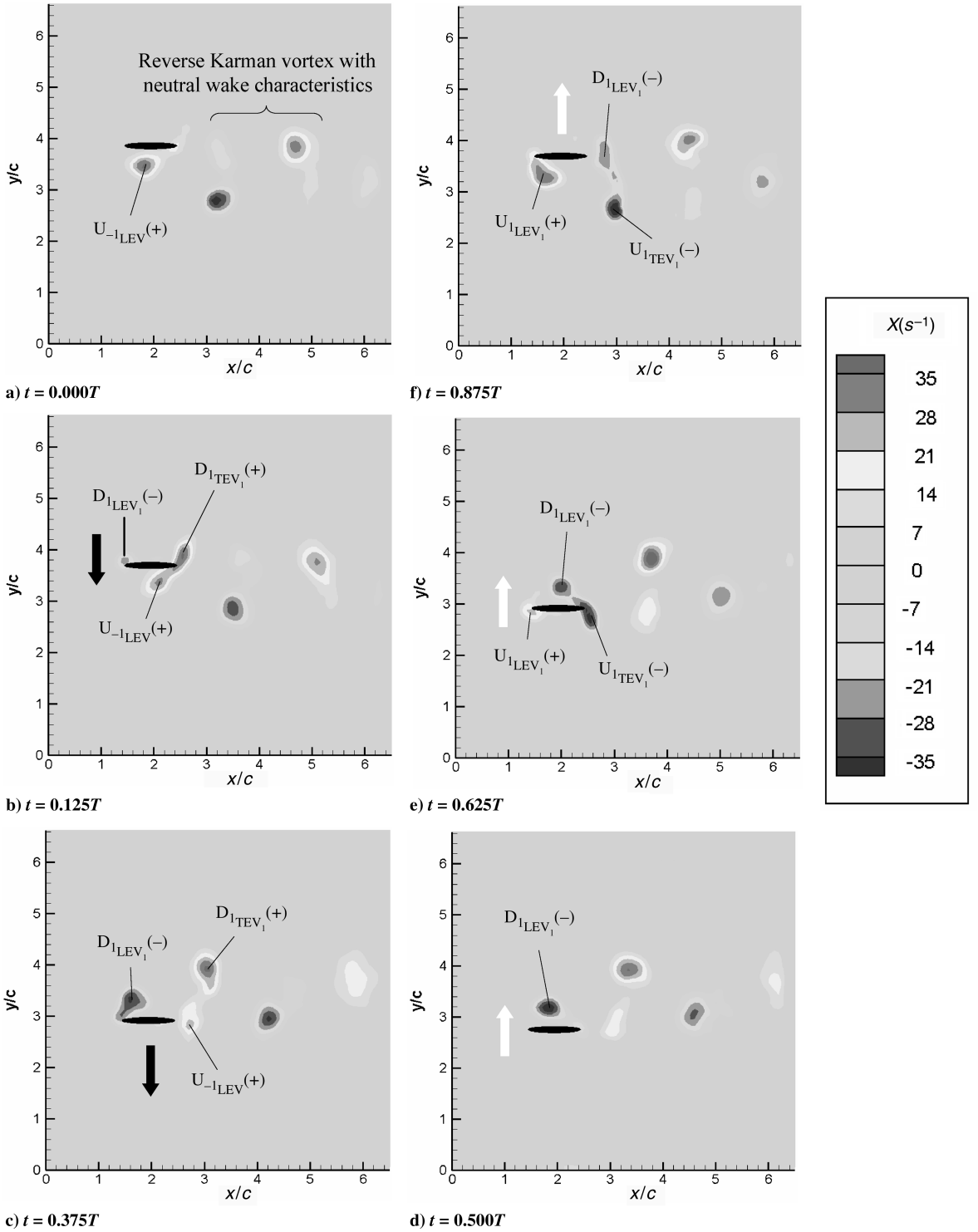

Fig. 8 Vorticity plot of $Sta = 0.276$ ($h = 0.552$) and $Stc = 0.5$ over one cycle of heaving motion (reverse-Kármán-vortex-street-like structure).

edge of the airfoil ($t = 0.750T$). At the end of the upstroke, the merged $D_{-1_{LEV}}(-) + U_{1_{TEV_1}}(-)$ had separated from the trailing edge and $U_{-1_{LEV}}$ had reached the trailing edge. The end result was the merged $U_{-2_{LEV}}(+) + D_{1_{TEV_1}}(+)$ interacting with the merged $D_{-1_{LEV}}(-) + U_{1_{TEV_1}}(-)$ to form two rows of vortices with the circulations that gave a reverse-Kármán-vortex-street-like structure. In this case, it can be seen that the top-row vortices were formed from the merging of the TEV of the current downstroke with the LEV of the upstrokes formed two cycles earlier. Similarly, the bottom-row vortices were formed from the merging of the TEV of the current upstroke with the LEV of the downstroke formed two cycles earlier. This characteristic is partly caused by the higher heaving frequency.

3. Deflected Wakes

At even higher frequencies ($Sta = 0.160$ at $Stc = 2.00$ and $Sta = 0.276$ at $Stc = 1.00$ and 2.00) deflected wakes are formed. Figure 6 shows the vorticity plot of $Sta = 0.276$ at $Stc = 1.00$. Here, as the airfoil moved downward, the TEV $[D_{1_{TEV_1}}(+)]$ shed from the trailing edge merged with the TEV $[U_{-1_{TEV}}(+)]$ formed during the upstroke one cycle earlier, to form a vortex pair or dipole, with the induced velocity vector inclined to the downstream direction. The direction of deflection is determined by the starting condition of the plunging oscillating airfoil, because when the direction of starting stroke of the heaving motion was reversed, the wake deflected in the mirror-image direction. The dominant effect of the starting condition on the

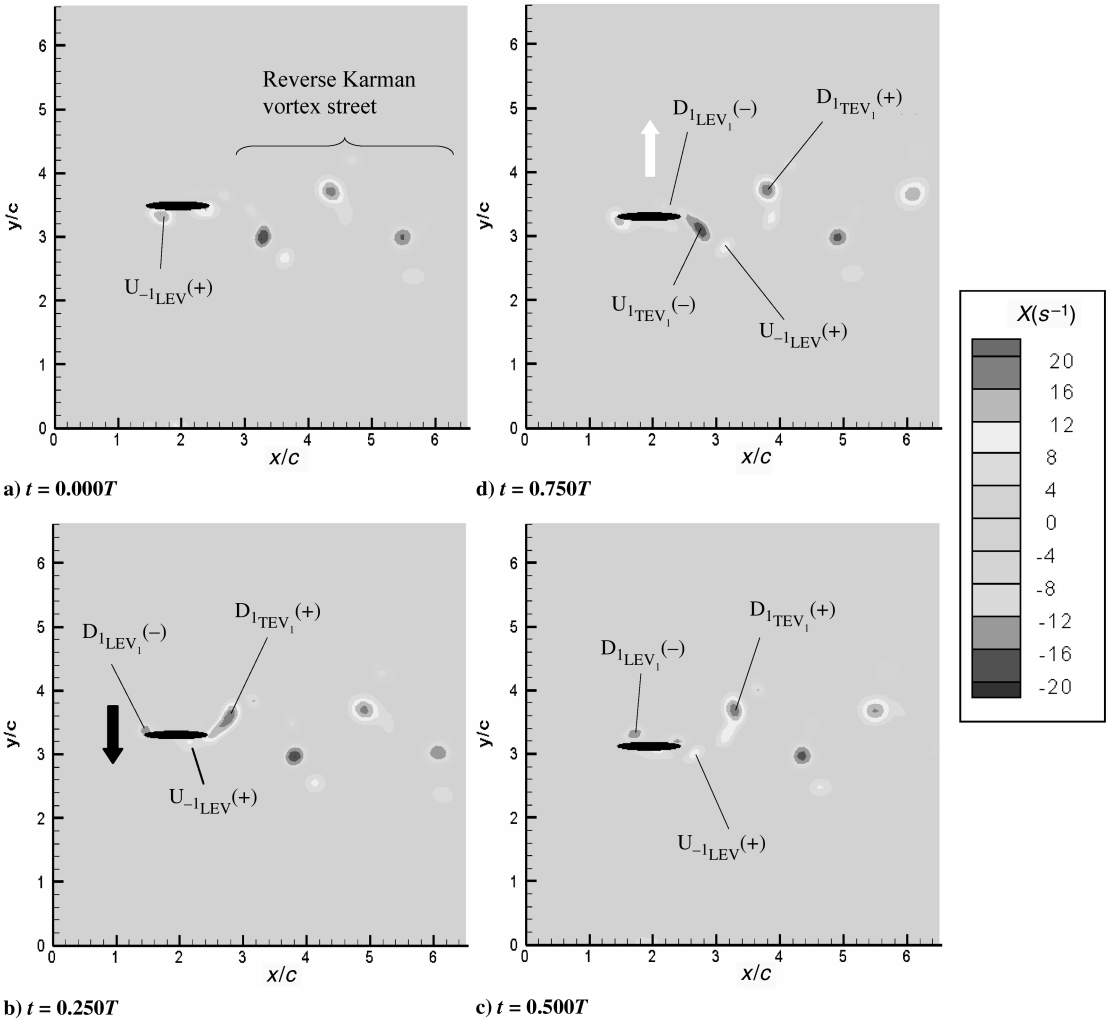

Fig. 9 Vorticity plot of $Sta = 0.0919$ ($h = 0.1838$) and $Stc = 0.5$ (reverse-Kármán-vortex-street-like structure).

direction of deflection was also observed in the numerical calculation by Jones et al. [48].

A combination of these vortex pairs gives the appearance of a deflected wake similar to that observed by LP [24] and LH [25]. Although these wake structures are produced from the LEV and TEV, a previous study [23] showed that they can also be produced from the shedding of the trailing-edge vortices only.

4. *Neutral Wake Structures*

These wake structures have also been previously observed by LP [24] and LH [25] and occur in the present experiment at lower frequency when *Stc* was around 0.50. At the beginning of every stroke, the LEV formed in the previous stroke did not merge with the newly formed TEV. Thus, a pair of vortices of the same sign was shed with every single stroke of the heaving motion.

Figure 7 shows the vorticity plot of $Stc = 0.50$ and $Sta = 0.160$. At $t = 0.000$, the LEV [$U_{-1_{LEV}}(+)$] formed during the previous upstroke was still attached to the airfoil, and as the airfoil moved downward, the $U_{-1_{LEV}}(+)$ convected toward the trailing edge. During this time, a TEV [$D_{1_{TEV_1}}(+)$] of the same sign was also generated and shed at the trailing edge (see $t = 0.125T$ and $0.250T$). A moment later at $t = 0.375T$, the $U_{-1_{LEV}}(+)$ was also shed into the wake and aligned almost vertically with $D_{1_{TEV_1}}(+)$. The process then repeated for the next half-cycle. Therefore, for every cycle of the heaving motion, the wake consisted of two pairs of vortices, with each pair having the same sign circulation. Close examination of the result shows that in every vortex pair, the LEV is slightly weaker than the TEV. This could be attributed to the combined effect of vortex stretching and vorticity diffusion as the LEV convected along the airfoil surface during the heaving motion. Because one vortex was stronger than the other, the induced velocity of the stronger TEV caused the weaker LEV to rotate around it, as can be seen further downstream.

In addition to the preceding configuration, the characteristics of the neutral wakes produced at $Stc = 0.50$ were found to vary with *Sta*. In particular, for the highest *Sta* of 0.276, because one vortex is significantly stronger than the other, the resulting wake pattern closely resembles that of a reverse Kármán vortex street, as can be seen in Fig. 8. From a thrust-producing viewpoint, this is definitely a reverse-Kármán-vortex-street structure, but the pattern is included here purely from a flow-topology consideration. During the experiment, it could be seen that every time the airfoil reversed its direction of motion, and because of the higher amplitude and velocity encountered here, the airfoil compressed the LEV ($U_{-1_{LEV}}$) produced during the previous stroke (see $t = 0.125T$), causing it to stretch and weaken rapidly before shedding from the trailing edge as a much weaker TEV (see $t = 0.375T$). Although the vortex pair looks like a neutral wake structure at the beginning, the weaker one diffused rapidly, and at about 1.5-chord length downstream from the airfoil, the wake resembles a reverse Kármán vortex street (see $t = 0.500T$). Note that in Fig. 11, this case is considered as a reverse-Kármán-vortex-street-like structure. When *Sta* was reduced to 0.0919 (see Fig. 9), the mechanism leading to the formation of a neutral wake structure, and its subsequently transformation into a reverse-Kármán-vortex-street appearance due to the demise of the weaker vortex is similar to that depicted in Fig. 8. Note that in Fig. 11, this case is also considered as a reverse-Kármán-vortex-street-like structure. The wake patterns shown in Figs. 8 and 9 would become the same pattern shown in Fig. 4 if merging of the

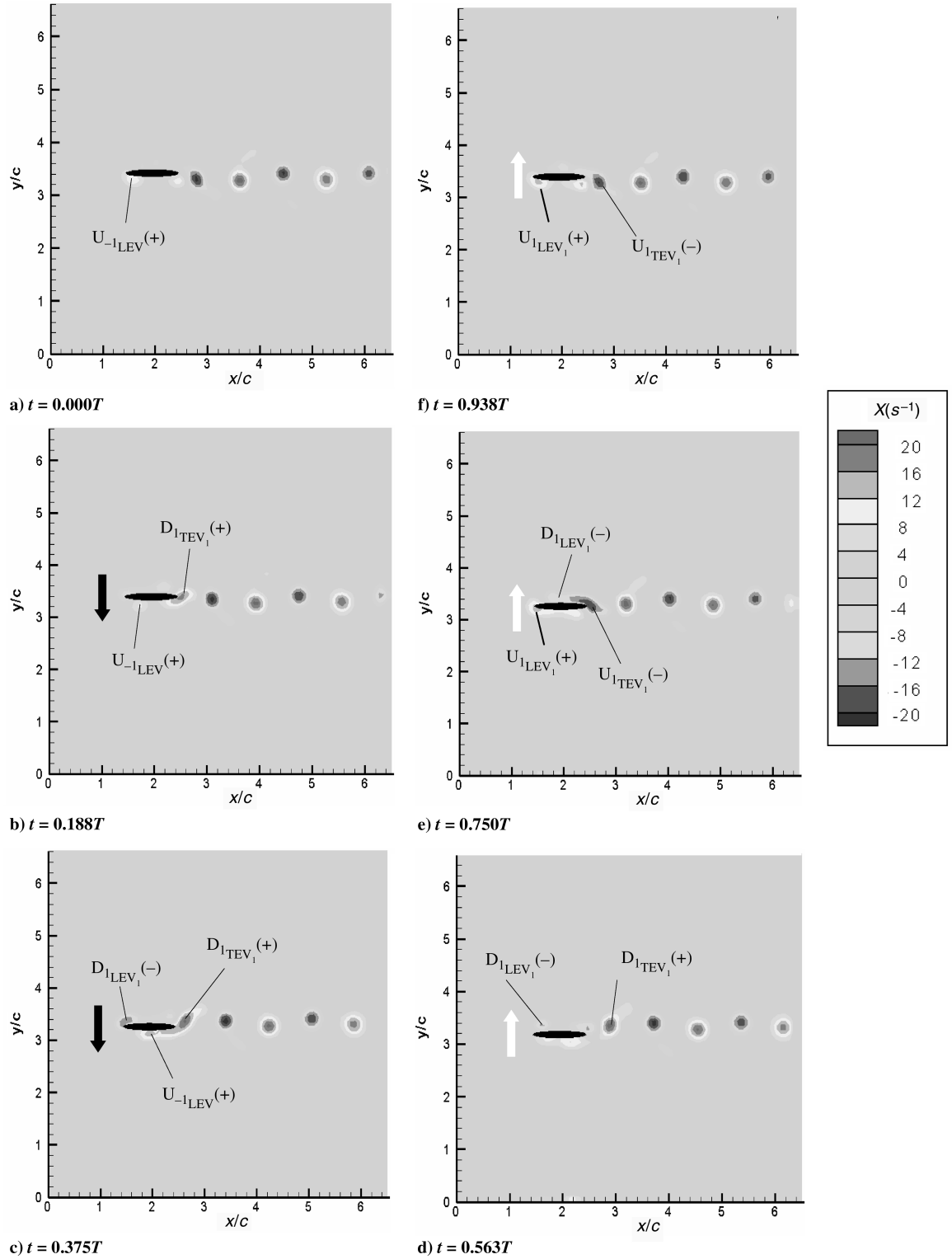

Fig. 10 Vorticity plot of $Sta = 0.0919$ ($h = 0.123$) and $Stc = 0.75$ over one cycle of heaving motion (merged Kármán vortex street).

like signs of the LEV and TEV had occurred at the beginning of every stroke.

5. Merged Kármán Vortex Street

At $Sta = 0.0919$ and $Stc = 0.75$, the results are presented in Fig. 10. Here, as the airfoil moved downward, it compressed the $U_{-1_{LEV}}(+)$ formed during the previous cycle and caused it to stretch. As a result, part of the vorticity was fed into $D_{1_{TEV_1}}(+)$ (see Figs. 10b and 10c). When the airfoil moved upward, a corresponding event occurred (see Figs. 10d–10f), resulting in the formation of a narrow line of vortex street. Close examination on the wake pattern reveals that the vortices arrange in a form of Kármán vortex street, although the lateral distance between the vortices is very small. It is thus called merged Kármán vortex street.

C. Discussion

A parameter map similar to that used by Triantafyllou et al. [21] and Jones et al. [23] to classify wake structures is presented in Fig. 11. The results of LH [25] (after converting into *Stc*, *Sta*, and *h*) are included for comparison. It should be noted that although LH conducted extensive computations on the heaving motion, we are able to ascertain only 11 cases, with 10 cases derived from the

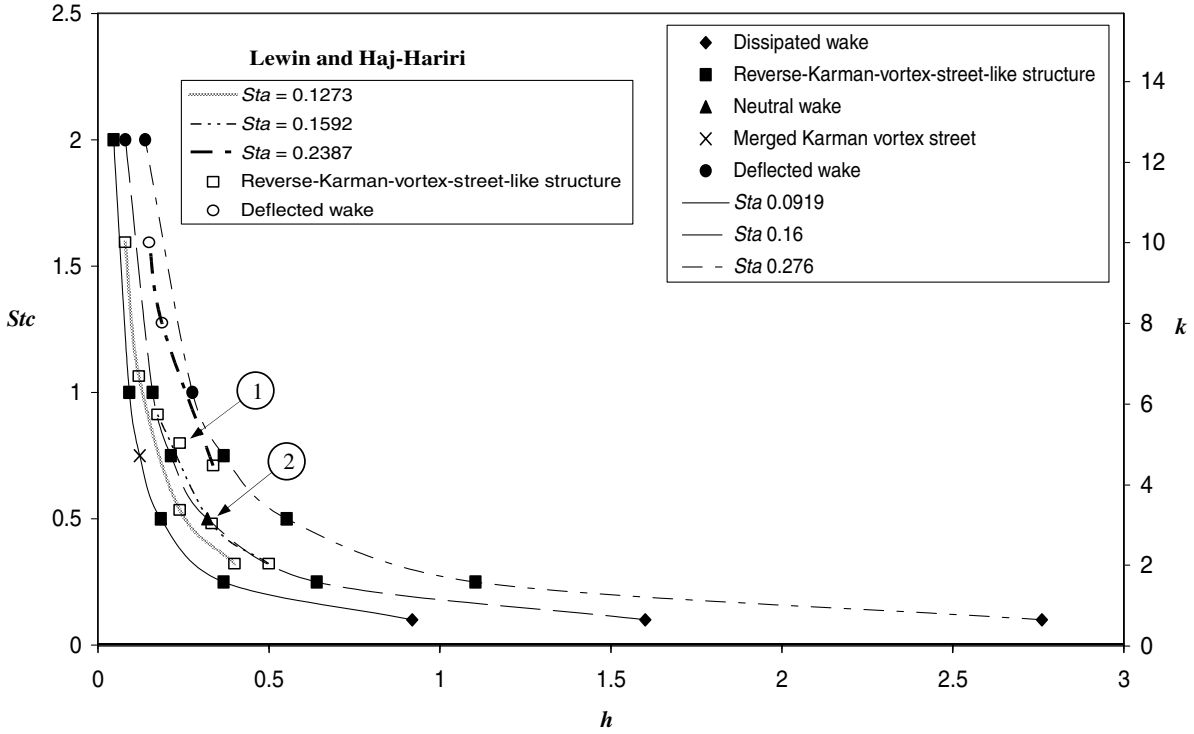

Fig. 11 A plot showing the dependency of wake structures on *Sta*, *Stc*, and *h*. Note that $Stc = k/2\pi$ and $Sta = kh/2\pi$. Open symbols represent the computation results of Lewin and Haj-Hariri [24], including the data for $Stc = 0.7958$ and $Sta = 0.191$ (identified as point 1 in the plot), which was not conducted in the present investigation. Solid symbols represent the present results. Note that at location 2, our experiment ($Stc = 0.5$ and $Sta = 0.16$) indicates a neutral wake, whereas the computation of Lewin and Haj-Hariri ($Stc = 0.477$ and $Sta = 0.1592$) indicates a reverse Kármán vortex street.

vorticity plots presented in their paper and one case based on their discussion of the result. For the remaining cases presented in Fig. 2 of their paper, it is difficult to ascertain the exact wake structures based on the data presented.

Within the confines of limited comparison, it can be seen from Fig. 11 that our results are in good agreement with that of LH [25]. For example, LH's results for $Sta = 0.2387$ shows the wake structure changing from a thrust-producing reverse-Kármán-vortex-street-like structure to deflected wakes as Stc is increased. A similar trend is displayed by our results at a slightly higher $Sta = 0.276$. Likewise, LH's results at $Sta = 0.1592$ show the presence of reverse-Kármán-vortex-street-like structures for a range of Stc, and our results at the same $Sta = 0.16$ also show the same wake structures for the same range of Stc, with the exception of point 2, which indicates a neutral wake (see Fig. 7). It is unclear why this is the case, even though the experiment and the computation are conducted at the same flow condition. Similarly, LH's results at $Sta = 0.1273$ also show the reverse-Kármán-vortex-street-like structure for a range of Stc, and our results at a lower $Sta = 0.0919$ also show the same wake structures for the same range of Stc, except at $Stc = 0.75$, which shows a Kármán vortex street (see Fig. 10). The reason for the difference is not clear to us, although our Sta value is about 28% lower. Note that LH's data for $Stc = 0.7958$ and $Sta = 0.191$ (identified as point 1) are also included in the plot for completeness, even though we did not conduct the experiment for this condition.

As Figs. 2–10 clearly show, the type of wake structures produced by a heaving 2-D elliptic airfoil depends primarily on when and how LEVs interact with TEVs. Although LP [24] observed all the wake structures reported here, except the dissipated wake for a heaving NACA 0012 airfoil, their flow structures appear to be originated from the trailing edge of the airfoil. Their finding is reinforced in a subsequent numerical study by Young and Lai [26] on a heaving NACA 0012 airfoil, which shows that although leading-edge separation appears to dominate aerodynamic forces for k (as defined in the present paper) less than eight, "wake structures appear to be controlled primarily by trailing-edge effect" for k up to 40. This raises the question as to why their results are different from that of LH [25] and the present study? An examination of the parameters used by LP shows that their airfoil was subjected to much smaller heaving amplitudes and higher frequencies. However, as can be deduced from our results in Figs. 9 and 10, high heaving frequency and low amplitude (i.e., high Stc and low Sta) will lead to weak LEVs due to partial annihilation of vorticity by the airfoil motion. With the NACA 0012 airfoil, the round leading edge of the airfoil further inhibits strong leading-edge flow separation. Therefore, the resultant reverse-Kármán-vortex-street structure is produced from the shedding of the trailing-edge vortices only. In contrast, much larger amplitudes of heaving are used in the present experiment (and also in LH's computations), and this combined with a sharper leading edge of the elliptic airfoil provides a more favorable condition for stronger flow separation, resulting in the formation of shed LEVs, which plays a crucial role in the wake formation. However, a recent thesis by Young [49] on numerical simulation of the unsteady aerodynamics of flapping airfoils shows that strong leading-edge vortices can also be shed from the NACA 0012 airfoil for certain parameter combinations; unfortunately, no experimental results are available to verify these predictions.

IV. Conclusions

The formation of the large-scale wake structures of a 2-D elliptic airfoil undergoing sinusoidally heaving motion at $Re = 1000$ was studied experimentally using digital particle image velocimetry technique. For the range of advance ratios and reduced frequencies investigated, five different wake structures are observed. In agreement with of the computations of LH [24], they are formed from the interaction of the LEV with the TEV and sometimes with the heaving airfoil. When the interaction leads to the merging of LEVs and TEVs, either a deflected wake or a drag-producing merged Kármán vortex street or a thrust-producing reverse-Kármán-vortex-street-like structure is produced. When no merging of LEVs and TEVs occurs, either a dissipated wake or neutral wake is formed. The type of wake structure produced depends on not only the advance ratio and the reduced frequency, but also the nondimensional heave amplitude.

Acknowledgments

The work was supported by the National University of Singapore through Academic Research Fund R-265-000-188-112.

References

[1] Knoller, R., "Die Gesetze des Luftwiderstandes," *Flug- und Motortechnik (Wien)*, Vol. 3, No. 21, 1909, pp. 1–7.
[2] Betz, A., "Ein Beitrag zur Erklaerung Segelfluges," *Zeitschrift für Flugtechnik und Motorluftschiffahrt*, Vol. 3, Jan. 1912, pp.269–272.
[3] Katzmayr, R., "Effect of Periodic Changes of Angle of Attack on Behavior of Airfoils," NACA TR TM 147, 1922 (translation from *Zeitschrift für Flugtechnik und Motorluftschiffahrt*).
[4] Glauert, H., "The Force and Moment on an Oscillating Airfoil," Aeronautical Research Council, R&M 1561, 1929.
[5] Garrick, I. E., "Propulsion of a Flapping and Oscillating Airfoil," NACA Report 567, 1936.
[6] Silverstein, A., and Joyner, U. T., "Experimental Verification of the Theory of Oscillating Airfoils," NACA Rept. 673, 1939.
[7] Von Kármán, T., and Burgers, J. M., "General Aerodynamics Theory-Perfect Fluids," *Aerodynamic Theory*, edited by W. F. Durand, Vol. 2, Springer, Berlin, 1943, p. 308.
[8] Bratt, J. B., *Flow Patterns in the Wake of an Oscillating Airfoil*, Aeronautical Research Council, R&M 2773, 1950.
[9] Wu, T., "Swimming of a Waving Plate," *Journal of Fluid Mechanics*, Vol. 10, No. 3, 1961, pp. 321–344.
[10] Lighthill, M. J., *Mathematical Biofluiddynamics*, Society for Industrial and Applied Mathematics, Philadelphia, 1975.
[11] Lighthill, M. J., "Hydromechanics of Aquatic Animal Propulsion," *Annual Review of Fluid Mechanics*, Vol. 1, 1969, pp. 413–446.
[12] Lighthill, M. J., "Aquatic Animal Propulsion of High Hydromechanical Efficiency," *Journal of Fluid Mechanics*, Vol. 44, No. 2, 1970, pp. 265–301.
[13] Chopra, M. G., "Hydromechanics of Lunate-Tail Swimming Propulsion," *Journal of Fluid Mechanics*, Vol. 64, No. 2, 1974, pp. 375–391.
[14] Chopra, M. G., "Large Amplitude Lunate Tail Theory of Fish Locomotion," *Journal of Fluid Mechanics*, Vol. 74, No. 1, 1976, pp. 161–182.
[15] Chopra, M. G., and Kambe, T., "Hydromechanics of Lunate Tail Swimming Propulsion, Part 2," *Journal of Fluid Mechanics*, Vol. 79, No. 1, 1977, pp. 49–69.
[16] Freymuth, P., "Propulsive Vortical Signatures of Plunging and Pitching Airfoils," *AIAA Journal*, Vol. 26, No. 7, 1988, pp. 881–883.
[17] Koochesfahani, M. M., "Vortical Patterns in the Wake of an Oscillating Airfoil," *AIAA Journal*, Vol. 27, No. 9, 1989, pp. 1200–1205.
[18] Ohmi, M., Coutanceau, M., Loc, T. P., and Dulieu, A., "Vortex Formation Around an Oscillating and Translating Airfoil at Large Incidences," *Journal of Fluid Mechanics*, Vol. 21, Feb. 1990, pp. 37–60.
[19] Ohmi, M., Coutanceau, M., Daube, O., and Loc, T. P., "Further Experiments on Vortex Formation Around an Oscillating and Translating Airfoil at Large Incidences," *Journal of Fluid Mechanics*, Vol. 225, Apr. 1991, pp. 607–630.
[20] Triantafyllou, M. S., Triantafyllou, G. S., and Gopalkrishnan, R., "Wake Mechanics for Thrust Generation in Oscillating Foils," *Physics of Fluids A*, Vol. 3, No. 12, 1991, pp. 2835–2837.
[21] Triantafyllou, G. S., Triantafyllou, M. S., and Grosenbaugh, M. A., "Optimal Thrust Development in Oscillating Foils with Application to Fish Propulsion," *Journal of Fluids and Structures*, Vol. 7, No. 2, 1993, pp. 205–224.
[22] Anderson, J. M., Streitlien, K., Barrett, D. S., and Triantafyllou, M. S., "Oscillating Foils of High Propulsive Efficiency," *Journal of Fluid Mechanics*, Vol. 360, Apr. 1998, pp. 41–72.
[23] Jones, K. D., Dohring, C. M., and Platzer, M. F., "Experimental and Computational Investigation of the Knoller–betz Effect," *AIAA Journal*, Vol. 37, No. 7, 1998, pp. 1240–1246.
[24] Lai, J. C. S., and Platzer, M. F., "Jet Characteristics of a Plunging Airfoil," *AIAA Journal*, Vol. 37, No. 12, 1999, pp. 1529–1537.
[25] Lewin, G. C., and Haj-Hariri, H., "Modelling Thrust Generation of a Two-Dimensional Heaving Airfoil in Viscous Flow," *Journal of Fluid Mechanics*, Vol. 492, Oct. 2003, pp. 339–362.
[26] Young, J., and Lai, J. C. S., "Oscillation Frequency and Amplitude Effects on Wake of a Plunging Airfoil," *AIAA Journal*, Vol. 42, No. 10, 2004, pp. 2042–2052.
[27] Milano, M., and Gharib, M., "Uncovering the Physics of Flapping Flat Plates with Artificial Evolution," *Journal of Fluid Mechanics*, Vol. 534, July 2005, pp. 403–409.
[28] Smith, M. J. C., Wilkin, P. J., and Williams, M. H., "The Advantages of an Unsteady Panel Method in Modeling the Aerodynamic Forces on Rigid Flapping Wings," *Journal of Experimental Biology*, Vol. 199, No. 5, 1996, pp. 1073–1083.
[29] Ellington, C. P., van den Berg, C., Willmott, A. P., and Thomas, A. L. R., "Leading-Edge Vortices in Insect Flight," *Nature (London)*, Vol. 384, No. 6610, 1996, pp. 626–630.
[30] Hall, K. C., and Hall, S. R., "Minimum Induced Power Requirements for Flapping Flight," *Journal of Fluid Mechanics*, Vol. 323, Sept. 1996, pp. 285–315.
[31] Willmott, A. P., and Ellington, C. P., "The Mechanics of Flight in the Hawkmoth Manduca Sexta, 1: Kinematics of Hovering and Forward Flight," *Journal of Experimental Biology*, Vol. 200, No. 21, 1997, pp. 2705–2722.
[32] Hall, K. C., Pigott, S. A., and Hall, S. R., "Power Requirements for Large-Amplitude Flapping Flight," *Journal of Aircraft*, Vol. 35, No. 3, 1998, pp. 352–361.
[33] Dickinson, M. H., Lehmann, F. O., and Sane, S. P., "Wing Rotation and the Aerodynamic Basis of Insect Flight," *Science*, Vol. 284, No. 5422, 1999, pp. 1954–1960.
[34] Wang, Z. J., "Vortex Shedding and Frequency Selection in Flapping Flight," *Journal of Fluid Mechanics*, Vol. 410, No. 1, 2000, pp. 323–341.
[35] Sane, S. P., and Dickinson, M. H., "The Control of Flight Force by a Flapping Wing: Lift and Drag Production," *Journal of Experimental Biology*, Vol. 204, No. 15, 2001, pp. 2607–2626.
[36] Taylor, G. K., Nudds, R. L., and Thomas, A. L. R., "Flying and Swimming Animals Cruise at a Strouhal Number Tuned for High Power Efficiency," *Nature (London)*, Vol. 425, No. 6956, 2003, pp. 708–711.
[37] Wu, J. H., and Sun, M., "Unsteady Aerodynamic Forces of a Flapping Wing," *Journal of Experimental Biology*, Vol. 207, No. 7, 2004, pp. 1137–1150.
[38] Parker, K., von Ellenrieder, K. D., and Soria, J., "Using Stereo Multigrid DPIV (SMDPIV) Measurements to Investigate the Vortical Skeleton Behind a Finite-Span Flapping Wing," *Experiments in Fluids*, Vol. 39, No. 2, 2005, pp. 281–298.
[39] Yamamoto, M., and Isogai, K., "Measurement of Unsteady Fluid Dynamic Forces for a Mechanical Dragonfly Model," *AIAA Journal*, Vol. 43, No. 12, 2005, pp. 2475–2480.
[40] Parker, K., von Ellenrieder, K. D., and Soria, J., "Thrust Measurement from a Finite-Span Flapping Wing Model," *AIAA Journal*, Vol. 45, No. 1, 2007, pp. 58–70.
[41] Perry, A. E., and Watmuff, J. H., "The Phase-Averaged Large-Scale Structures in 3-Dimensional Turbulent Wakes," *Journal of Fluid Mechanics*, Vol. 103, Feb. 1981, pp. 33–51.
[42] Cantwell, B. J., and Coles, D., "An Experimental-Study of Entrainment and Transport in the Turbulent Near Wake of a Circular-Cylinder," *Journal of Fluid Mechanics*, Vol. 136, Nov. 1983, pp. 321–374.
[43] Perry, A. E., and Steiner, T. R., "Large-Scale Vortex Structures in Turbulent Wakes Behind Bluff-Bodies, Part 1: Vortex Formation Process," *Journal of Fluid Mechanics*, Vol. 174, Jan. 1987, pp. 233–270.
[44] Kelso, R. M., Lim, T. T., and Perry, A. E., "An Experimental Study of Round Jets in Cross-Flow," *Journal of Fluid Mechanics*, Vol. 306, Jan. 1996, pp. 111–144.
[45] Luff, J. D., Drouillard, T., Rompage, A. M., Linne, M. A., and Hertzberg, J. R., "Experimental Uncertainties Associated with Particle Image Velocimetry (PIV) Based Vorticity Algorithms," *Experiments in Fluids*, Vol. 26, No. 1–2, 1999, pp. 36–54.
[46] Cohn, R. K., and Koochesfahani, M. M., "The Accuracy of Remapping Irregularly Spaced Velocity Data onto a Regular Grid and the Computation of Vorticity," *Experiments in Fluids*, Vol. 29, No. 7, Dec. 2000, pp. S61–S69.
[47] Morikawa, K., and Gronig, H., "Formation and Structure of Vortex Systems Around a Translating and Oscillating Airfoil," *Zeitschrift fur Flugwissenschaften und Weltraumforschung*, Vol. 19, No. 6, 1995, pp. 391–396.
[48] Jones, K. D., Dohring, C. M., and Platzer, M. P.F, "Wake Structures Behind Plunging Airfoils: A Comparison of Numerical and Experimental Results," AIAA Paper 96-0078, Jan. 1996.
[49] Young, J., "Numerical Simulation of the Unsteady Aerodynamics of Flapping Airfoils," Ph.D. Thesis, School of Aerospace, Civil and Mechanical Engineering, Univ. of New South Wales, Australian Defence Force Academy, Canberra, Australia, 2005.

K. Fujii
Associate Editor